Which Pattern? Biasing Aspects of Planar Calibration Patterns and Detection Methods

John Mallon *   Paul F. Whelan

Vision Systems Group, Dublin City University, Dublin 9, Ireland

Abstract

This paper provides a comparative study on the use of planar patterns in the generation of control points for camera calibration. This is an important but often neglected aspect in camera calibration. Two popular checkerboard and circular dot patterns are each examined with two detection strategies for invariance to the potential bias from projective transformations and nonlinear distortions. It is theoretically and experimentally shown that circular patterns can potentially be affected by both biasing sources. Guidelines are given to control such bias. In contrast, appropriate checkerboard detection is shown to be bias free. The findings have important implications for camera calibration, indicating that well accepted methods may give poorer results than necessary if applied naively.

Key words: Camera Calibration, Calibration Patterns, Bias Compensation, Lens Distortion.

1 Introduction

There is an abundance of planar charts used within the realms of camera calibration as sources of both 2D and 3D control points. These points are generally constructed on a planar surface by means of some high contrast pattern. In turn, the pattern also facilitates the recovery of the control point projections on the image plane. Patterns such as squares (Zhang, 2000; Weng et al., 1992), checkerboards (Lucchese and Mitra, 2002) and circles (Heikkila, 2000; Asari et al., 1999; Kannala and Brandt, 2006) have become popular as they can be readily manufactured to a sufficient precision, and their data points are recoverable through the use of standard image processing techniques.

---

* Corresponding author. Tel.: +353 1 7005869 Fax: +353 1 7005508
  Email address: john.mallon@eeng.dcu.ie (John Mallon).

In real cameras, an image of the calibration pattern is likely to undergo two types of transformation: a projective transformation as a consequence of relative 3D position, and a nonlinear transformation due to various lens distortions. The control point invariance to errors resulting from these two transformations is based on a combination of the pattern employed, and the detection method used. As a consequence, for any theoretical combination of calibration pattern and detection method, we have identified two possible sources of bias in control point recovery, which we simply term: Perspective bias and Distortion bias. In practice, the presence of these bias sources is primarily governed by the type of pattern used, which in turn dictates the appropriate detection methods. This study is based on two calibration patterns from the camera calibration literature, each with two associated control point detection strategies. These are the popular checkerboard and circular dot patterns with the standard detection strategies of edge intersections, corners, centroids and conic fitting. The underlying biasing principles naturally extend to other similar patterns and detection methods. The importance of acquiring bias free data has often been ignored in calibration articles, the result being that camera models and accuracy cannot be reliably evaluated.

Naturally, many studies in camera calibration have focused specifically on achieving high calibration accuracy and stability. These works are primarily founded on high precision control points of either 2D or 3D variety, and the accurate detection of their projections. Linear least-square techniques for calibration are improved upon by Tsai (1987) and Weng et al. (1992), who concentrate on improving the calibration accuracy by comprehensively modelling lens distortion and further iteratively optimising the parameters. A comparative study is presented in Salvi et al. (2002). Planar calibration techniques have been proposed by Strum and Maybank (1999) and Zhang (2000) that place the world coordinate system on the calibration object and thus require only arbitrarily scaled 2D coordinates. These methods, requiring less arduous control point specifications, have contributed largely to the common adoption of planar calibration targets. These works assume that the detected image points have zero mean gaussian distributions in order to correctly converge to the optimal solution. This may not always be the case. Heikkila (2000) and Kannala and Brandt (2006) describe calibration techniques using circular control points including corrections for their perspective bias to improve the calibration accuracy.

Our main aim is to aid the practitioner to establish which pattern, and what design offers, the best precision in control point recovery. The primary concern in this regard is to obtain bias free data, as this is clearly essential for obtaining uncorrupted estimates from calibration algorithms. We show theoretically and experimentally, with both real and simulated data, that control points detected using the centroid recovery principle, can potentially be corrupted by both perspective bias and distortion bias, with the likelihood of greater

2

distortion bias magnitude in a typical camera. However, only perspective bias compensation has been considered in the literature, using adjusted conic centroids. It is shown that the compensation of distortion bias from such circular pattern points is not possible without first knowing the distortion. Also, the bias magnitudes resulting from the standard least square conic fitting are shown to be much less in comparison. This informs a set of basic guidelines for use with circular type patterns to minimise the introduction of such biases. In contrast, checkerboard patterns with certain detection strategies, are shown to be inherently bias free. Overall, this study highlights that even well-accepted calibration methods may give poorer results than necessary if applied naively through the use of inappropriate pattern design.

Our analysis is primarily conducted on simulated images with known ideal control points. Images and control points are synthesised with both nonlinear and projective transformations. Details of the image synthesis precision is presented ensuring no additional errors are introduced from this stage. We concentrate on automatic point recovery where all points are observable in the image. Two standard sub-pixel detection strategies for each pattern are described, each having unique bias invariant properties. The sources of biases are theoretically identified for each pattern and are subsequently verified on the simulated images. A comparative study of each method with respect to blurring and noise serves to show that the biasing magnitudes are significantly greater than the expected detection accuracy or noise floor. Finally, examples of distortion bias in a real images are shown. Overall, this paper emphatically shows that the choice of pattern and detection technique is much more important than previously realised to achieve bias free control points for real cameras affected by lens distortion.

2   Pattern and control point synthesis

Two factors influence the recovery of control points: the camera lens effects and the relative positioning of the calibration object. The error invariance to these transformations is based on the type of pattern employed and the detection strategy used. Two popular patterns are chosen for this study, each with sufficiently different characteristics to illustrate all the possible sources of control point bias. Biasing aspects of other pattern types can be understood by comparison with the principles introduced here. The chosen checkerboard and circular patterns are illustrated in canonical form in Fig. 1. The sizes of the circles and checkerboard squares, and the actual number of control points are chosen as typical practical values. For our analysis we subject each pattern to gaussian blurring, additive gaussian noise, pincushion and barrel distortion and random placements. The recovered points are then be compared with their true locations. For the distortion and positioning effects, both control
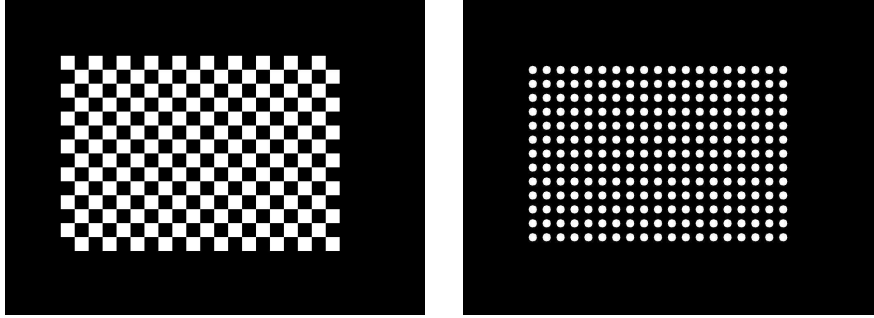
Fig. 1. The two classes of patterns used for this study, checkerboard and circles, shown in their canonical form. Image dimensions are 2560 x 1920 pixels. 247 control points are synthesised. Checkerboard squares have dimensions 85 x 85 pixels, while circle diameters are 51 pixels. The center or principle point is at (1280,960).

points and the corresponding image must be transformed. Geometric image re-sampling is carried out by mapping from the transformed image to the original. This involves calculating for every pixel in the transformed image, the corresponding pixel coordinate in the original image, effectively requiring an inverse mapping. The transformed image intensity is then calculated based on the standard bilinear interpolation around this coordinate.

2.1 Pattern positioning

The image perception of various 3D positions of the control points, $\mathbf{p} = (x, y, 1)^T$, (in homogeneous form) are simulated using a pseudo randomly generated homography $\mathbf{H}$, giving $\mathbf{p} = \mathbf{H}\bar{\mathbf{p}}$, where $\bar{\mathbf{p}}$ are the canonical representation of the control points. This homography is generated by a combination of a 3D rotation and translation, whose values are drawn randomly from a specific range. This range limit ensures that the transformed image lies roughly within the image window and that its apparent 3D position simulates a likely view of the calibration object. The corresponding image re-sampling is calculated using $\mathbf{H}^{-1}$.

We also need a means of quantifying a perspective transformation in terms of how close it is to being a similarity. Taking the third row of the transformation on its own does not provide sufficient information as this does not consider the affine element of the projective transform. It has been demonstrated in Mallon and Whelan (2005) that the affine element of a homography directly influences its perspective properties. Therefore the homography as a whole must be considered. One useful way to do this is to employ matrix norms, ideally giving a single valued measure of severity of the perspective aspect. However, as the transform is inherently non-linear these cannot be directly applied. To over-

4

come this we consider the norms of the transform's Jacobian, in particular the largest largest singular value (L_2 norm) divided by the smallest. Ideally both singular values are equal giving a condition of one. The condition number is then:

$$\text{cond}(\mathbf{J}(\mathbf{H},\mathbf{p})), \quad \text{where} \quad \mathbf{J}(\mathbf{H},\mathbf{p}) = \begin{pmatrix} \frac{\partial x}{\partial \bar{x}} & \frac{\partial x}{\partial \bar{y}} \\ \frac{\partial y}{\partial \bar{x}} & \frac{\partial y}{\partial \bar{y}} \end{pmatrix}.$$

This linearly quantifies the local perspective effects of the nonlinear transformation at points $\mathbf{p}$ within the image window. The mean of these values is taken as the net effect of the perspective transform.

2.2 Simulating lens distortion

General radial lens distortion is approximated in an image by: (Born and Wolf, 1980; Mallon and Whelan, 2007)

$$\check{\mathbf{p}} = \mathbf{p} + \mathcal{D}(\mathbf{p},\mathbf{k}), \quad \text{where} \quad \mathcal{D}(\mathbf{p},\mathbf{k}) = \begin{pmatrix} x(k_1 r^2 + k_2 r^4 + 1) \\ y(k_1 r^2 + k_2 r^4 + 1) \end{pmatrix}, \qquad (1)$$

where $\mathbf{p} = (x,y,1)^T$ are the undistorted image coordinates with $r^2 = x^2 + y^2$ and $\check{\mathbf{p}} = (\check{x},\check{y},1)^T$ are the corresponding distorted coordinates. More details on the origins of this model are given in Mallon and Whelan (2007). The distortion parameter, (k_1), is used as an index, with values varying through $\pm 2(pix^3)$, with $k_2 = -k_1$. These values are applied to pixel coordinates normalised by the average of the image width and height, denoted by (pix). In order to re-sample a distorted image an inverse of (1) is required. We use the approximate model proposed in Mallon and Whelan (2004) :

$$\mathcal{D}^*(\check{\mathbf{p}},\delta) = \begin{pmatrix} \check{x}(\delta_1 \check{r}^2 + \delta_2 \check{r}^4 + \delta_3 \check{r}^6 + \delta_4 \check{r}^8 + 1) \\ \check{y}(\delta_1 \check{r}^2 + \delta_2 \check{r}^4 + \delta_3 \check{r}^6 + \delta_4 \check{r}^8 + 1) \end{pmatrix} / (1 + 4\delta_5 \check{r}^2 + 6\delta_6 \check{r}^4). \quad (2)$$

The parameters of this model are linearly estimated using a dense collection of points covering the image window. The inversion accuracy for the distortion range under consideration is shown in Table 1. These residuals are orders of magnitude lower than the precision of the sub-pixel point detection algorithms, (see section 4), ensuring that no additional source of error is introduced from the simulated images.

Table 1
Inverse distortion residuals after the fitting of equation 2. Levels are orders of magnitude below that of the control point detection accuracy, see section 4

k_1 (Barrel)	-2	-1.75	-1.5	-1.25	-1	-0.75	-0.5	-0.25
Mean $\times 10^{-5}$	0.6997	1.8487	0.4540	0.1080	0.0051	0.0095	0.0027	0.0007
SD $\times 10^{-4}$	1.7838	0.9531	0.1255	0.0232	0.0013	0.0015	0.0003	0.0001
k_1 (Pincushion)	0.25	0.5	0.75	1	1.25	1.5	1.75	2
Mean $\times 10^{-5}$	0.0001	0.0028	0.0192	0.0735	0.2045	0.4682	0.9425	1.4668
SD $\times 10^{-4}$	0.0000	0.0001	0.0012	0.0051	0.0151	0.0372	0.0806	1.0379

3 Control point recovery

For each pattern, two general sub-pixel detection strategies are described. These strategies are chosen for their unique biasing properties. Unfortunately, it is impossible to completely generalise the detection methods, so where necessary the implementation details are provided. In this sense, e.g. regardless of what type of edge detector, thresholds, etc. are used, the principles may be easily abstracted to other detection strategies and patterns. The circle detection methods are based on the centroid extraction and ellipse fitting. Square detection methods are based on refining an initial corner solution with edge intersections and with local surface fitting. It will be shown that the detection methods are subject to two sources of biasing. We theoretically show how they arise as a result of perspective viewing and lens distortion.

3.1 Circle pattern detection

Given an image of a circular pattern, and following a suitable thresholding operation, the centroids of the circles are simply calculated as:

$$
\mathbf{c_{cen}} = (x_{cen}, y_{cen}, 1)^T = \left(\frac{\sum_{x_f \in F} x_f \cdot I(\mathbf{p_f})}{\sum_{x_f \in F} I(\mathbf{p_f})}, \frac{\sum_{y_f \in F} y_f \cdot I(\mathbf{p_f})}{\sum_{y_f \in F} I(\mathbf{p_f})}, 1 \right)^T, \quad (3)
$$

where $I(\mathbf{p_f})$ is the intensity at point $\mathbf{p_f}$ (binary in practice) and F is the set of pixels deemed to belong to the circle. Equivalently, the first and second order shape moments can be used. Note that our simulated images suffer no illumination variations[1]. It is known that if the calibration plane is not parallel with the image plane, a bias is introduced into $\mathbf{c_{cen}}$.

---

[1] When dealing with real images, the illumination and vignetting effects must be countered with techniques such as careful local thresholding to avoid introducing additional bias.

3.1.1 Perspective bias

Considering a calibration plane in a general 3D position, a homography $\mathbf{H}$ can be computed between the pixel coordinates of the control points and the ideal canonical position as: $\mathbf{p} = \mathbf{H}\bar{\mathbf{p}}$, where $\mathbf{p}$ are the locations of the control points in the image, and $\bar{\mathbf{p}}$ are the ideal canonical position of the control points. The conic approximation to the edge points of the pattern, $\bar{\mathbf{p}}_{edge}$, can be estimated linearly as: $\bar{\mathbf{p}}_{edge}^T \bar{\mathbf{Q}} \bar{\mathbf{p}}_{edge}$ (Hartley and Zisserman, 2003). The center of the conic is then calculated as: $\bar{\mathbf{c}}_{conic} = \bar{\mathbf{Q}}^{-1}(0,0,1)^T$. For a general 3D position these centers transform to $\mathbf{c}_{conic} = \mathbf{H}\bar{\mathbf{Q}}^{-1}(0,0,1)^T$. However, in an image only the conic $\mathbf{Q}$ is available, but this is related to $\bar{\mathbf{Q}}$ through $\mathbf{Q} = \mathbf{H}^{-T}\bar{\mathbf{Q}}\mathbf{H}^{-1}$. Thus the unbiased estimates for the centers of the conics undergoing a general perspective transform $\mathbf{H}$ is given by:

$$\mathbf{c}_{conic} = \mathbf{Q}^{-1}\mathbf{H}^{-T}(0,0,1)^T. \tag{4}$$
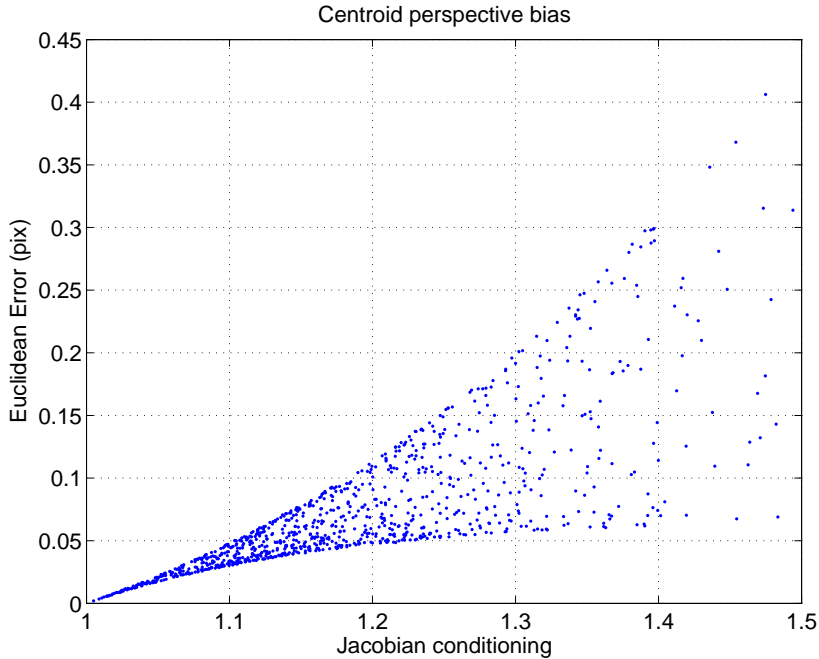
Fig. 2. Mean Euclidean error as a consequence of 1000 random positions of the circular pattern. Orthogonal like homographies induce a low conditioning (close to one) while the perspective bias increases with increasing conditioning.

The extent of this biasing influence is simulated in Fig. 2 for random perspective views described in section 2.1. In many algorithms, especially when lens distortion is a factor, the value of $\mathbf{H}$ or equivalently, the elements of the camera projection matrix, are not known exactly beforehand. This forces the algorithm to iteratively update the estimates of the control points. This

re-estimation of the control points is a serious complication, increasing the number of iterations and degrading derivative information.

3.1.2 Distortion bias

The second major drawback of circle patterns and their detection methods, is that they are also subject to bias from lens distortion. Lens distortion introduces a nonlinear shape warping to the area of the conic. This warping subsequently biases the center point of the conic. The extent of the bias is dependent on the amount of lens distortion and the area or radius of the conic, as illustrated in Figs. 3 and 4.
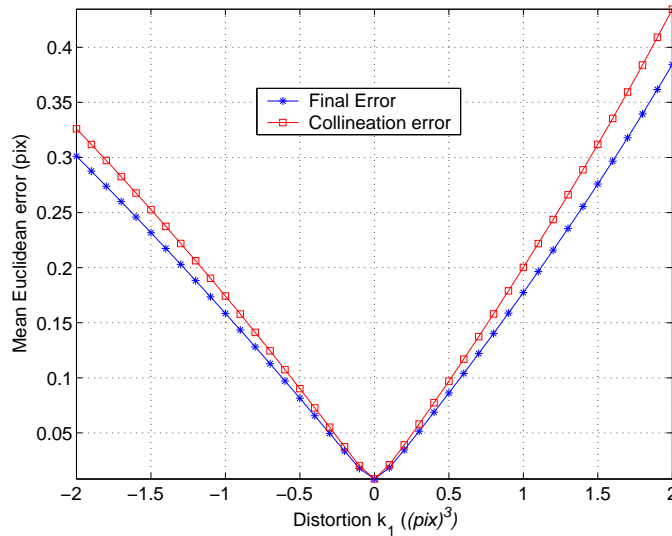
Fig. 3. Simulated mean Euclidean distortion bias for circle pattern (circle dia 50 pix) over the considered range of distortion. The collineation error resulting from $\mathbf{H}_{\mathcal{D}}$ is actually reduced by the conic ill-fitting error.

This bias results from the combined effects of two error sources. Firstly, the nonlinear nature of distortion (1) warps the conic so that it is no longer a true conic. Certain sections of the conic become elongated or compressed, all culminating in the introduction of a bias from the eventual conic fitting. Tracking the equations for only one term of distortion (k_1) the second order least squares conic fitting (i.e minimisation of an algebraic distance): $\mathbf{\breve{p}}^T\mathbf{\breve{Q}}\mathbf{\breve{p}}$, is performed on a sixth order section. This leads to an ill-fitting bias, the extent of which is illustrated in Fig. 3. The analytical compensation for such bias is not possible without exact knowledge as to the true undistorted state of the control points.

The second error source is from the distortion induced local perspective transform, resulting from the conic fitting. This can be visualised, for example, by taking two circular control points, one at the image center and the other

8
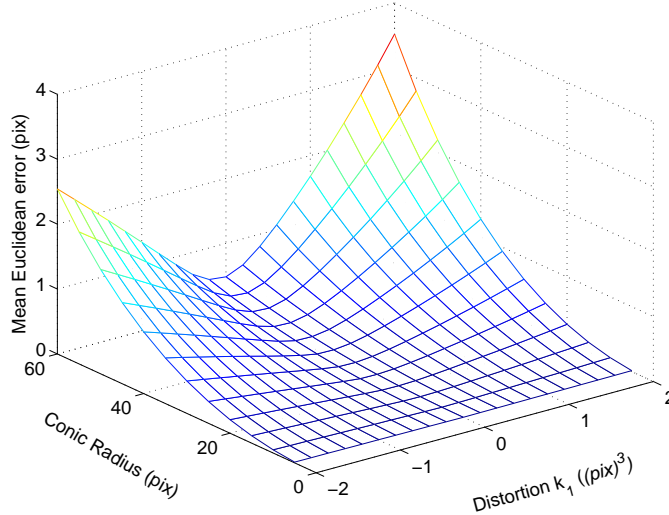
Fig. 4. Simulated mean Euclidean distortion bias in patterns of various circle radii, considered over a range of distortion levels.

somewhere around the perimeter where the distortion is severe. It can be noticed that, compared to the central point, the outer control point seems to be at positioned at a different relative position. This difference in perspective induces a bias as before, only now each control point is individually afflicted, depending on its location within the image. We call this a collineation error.

Considering a general distortion free conic $\mathbf{Q}$, its least square counterpart in distorted space is calculated by minimising the algebraic expression: $\sum_i (\breve{\mathbf{p}}_i, \breve{\mathbf{Q}}\breve{\mathbf{p}}_i)^2$, where $\breve{\mathbf{Q}}$ must be a real proper conic. These two conics are related through a set of collineations or homographies $\mathbf{H}_\mathcal{D}$ that map $\mathbf{Q}$ to $\breve{\mathbf{Q}}$ through $\mathbf{H}_\mathcal{D}^T \mathbf{Q} \mathbf{H}_\mathcal{D} = \breve{\mathbf{Q}}$. This collineation may be found by taking the orthogonal matrices $\mathbf{U}$ and $\breve{\mathbf{U}}$ that diagonalise $\mathbf{Q}$ and $\breve{\mathbf{Q}}$: $\mathbf{U}^T \mathbf{Q} \mathbf{U} = \mathbf{\Lambda}$ and $\breve{\mathbf{U}}^T \breve{\mathbf{Q}} \breve{\mathbf{U}} = \breve{\mathbf{\Lambda}}$, where $\mathbf{\Lambda} = diag(\lambda_1, \lambda_2, \lambda_3)$ and $\breve{\mathbf{\Lambda}} = diag(\breve{\lambda}_1, \breve{\lambda}_2, \breve{\lambda}_3)$, and by choosing $\mathbf{\Lambda_0} = diag(\sqrt{\breve{\lambda}_1/\lambda_1}, \sqrt{\breve{\lambda}_2/\lambda_2}, \sqrt{\breve{\lambda}_3/\lambda_3})$. The collineation $\mathbf{H}_\mathcal{D}$ is then formed as $\mathbf{H}_\mathcal{D} = \breve{\mathbf{U}} \mathbf{\Lambda_0} \mathbf{U}$. However, the equation $\mathbf{H}_\mathcal{D}^T \mathbf{Q} \mathbf{H}_\mathcal{D} = \breve{\mathbf{Q}}$ is not unique as it provides only five of the necessary eight independent constraints. For simulation purposes a unique solution is obtained in least square sense by minimising $\sum_i (\breve{\mathbf{p}}_i, \mathbf{H}_\mathcal{D} \mathbf{p}_i)^2$.

The homography $\mathbf{H}_\mathcal{D}$ introduces a local perspective bias that we call the collineation error. Compensation for this bias cannot be directly applied in real cameras as the undistorted points are always unobservable. The contribution of collineation error source is simulated in Fig 3, revealing that it is dominant, and is actually reduced by the ill-fitting error. Naturally, distortion bias is heavily dependent on the size of the feature. This is examined in Fig. 4 for a range of distortion levels and circle diameters. Comparing with the perspective bias simulated in Fig. 2, a typical low focal length lens, where k_1 is roughly in the region of $-0.3 \rightarrow -0.7 pix^3$, distortion bias is likely to be

9

greater in magnitude than perspective bias. This is verified in section 4. Note also that distortion bias is not limited to conic fitting, and is present to the same extent regardless of detection mode, centroids or conic fitting. Fig. 4 also demonstrates that the effect of bias for circular dot patterns is negligible if the pixel diameter of the dot is roughly less than ten pixels. This value should be used as a rule of thumb for optimal performance of a circular type pattern.

For the practitioner, it is always recommended to use sub-pixel conic boundaries and bias-free conic estimation procedures. As mentioned, standard Least Square (algebraic distance) fitting is employed with non sub-pixel boundaries in this paper. It is well known that this also induces a bias (Zhang, 1997). However, using this linear technique gives an insight into the relative scales of these conic estimation biases in comparison with the distortion and perspective biases. It can be seen (also consult Section 4) that the conic estimation bias is much smaller than the potential perspective and distortion bias. Thus, in practice, when using circular type patterns, priority should be given to the perspective and distortion bias sources. The hierarchy of potential bias sources is then: those emanating from lens distortion, those from perspective distortion and lastly from erroneous conic fitting.

3.2 Checkerboard pattern detection

Given an image of a checkerboard pattern, initial estimates of the location of the intersections can be gathered using standard corner detection methods (Jain et al., 1995). These estimates are generally within a few pixels of the true locations. We describe two existing means of refining these initial solutions using edge information (Willson, 1994; Li and Lavest, 1996) and surface fitting (Lucchese and Mitra, 2002). We do not address the filtering of points that do not belong to the pattern (filtering details can be found in Mallon and Whelan (2007)), or the ordering of data for subsequent comparisons.

3.2.1 Edge intersections

A fitting function that models line intersections is formulated. In order to use it with a checkerboard pattern the edges or intensity derivatives in a medium sized local region Ψ, centered on the initial estimate are first calculated. The function is then fit using non-linear iterative techniques:

$$\min_{\mathbf{h}} \| h_1 e^{-h_2^2((x-h_5)\cos h_3 + (y-h_6)\sin h_3)^2} + h_1 e^{-h_2^2((x-h_5)\sin h_4 + (y-h_6)\cos h_4)^2}$$

$$-2h_1 e^{-h_2^2((x-h_5)^2 + (y-h_6)^2)} - \Psi(x,y)\|^2 \ ,$$

10

where the intersection point is (h_5, h_6), h_1 is the height of the derivative profile, h_2 is the width of the profile and h_3 and h_4 are the edge directions. The process is illustrated in Fig. 5. As lines project to lines under perspective transformations, this detection method is invariant to perspective bias. However, under lens distortion, it is clear that lines project to curves, with the result that this method is affected by distortion bias. Consequently, an analytical proof is not perused.
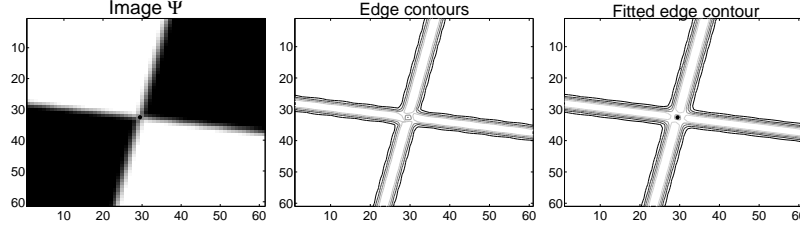
Fig. 5. Control point refinement based on edge fitting. The first image shows the selected ROI. Middle image shows the edge image contours. The final image shows the function fit contours from which the control point is calculated.

3.2.2 Corners
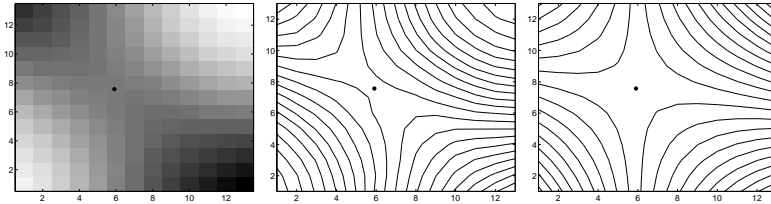
Fig. 6. The saddle refinement process. First the blurred ROI with marked saddle point is shown. Middle image is a contoured image of the intensity profile. Last image shows the intensity profile of the surface fit from which the saddle point is calculated.

A category of sub-pixel refinement is based on surface fitting of intensity around a corner point (Lucchese and Mitra, 2002). For each initial location estimate, a small region of interest Ψ is considered for fitting. Following blurring, a quadratic function can be linearly fit to the resulting intensity profile, as demonstrated in Fig. 6 by minimising:

$$\min_{\mathbf{s}} \|s_1 x^2 + s_2 xy + s_3 y^2 + s_4 x + s_5 y + s_6 - \Psi(x, y)\|^2.$$

The intersection point or saddle point is derived from this surface as the intersection of the two lines $2s_1 x + s_2 y + s_4 = 0$ and $s_2 x + 2s_3 y + s_5 = 0$. In practice, the small patch Ψ can effectively be considered a single point, especially in light of the detection accuracy and noise floor. As points project to points

11

under both projective and lens distortion transformations, this method has the desirable properties of being invariant to both perspective and distortion bias.

4 Experiments

Three sets of experiments are conducted on the synthesised test images described in section 2. The sizes of the circular patterns and chessboard are the same as those detailed in Figure 1. Two of the experiments verify and quantify the perspective and distortion bias for each detection method and pattern. A side by side accuracy evaluation for noise and blurring is presented, to give a benchmark from which to access the magnitude of both bias sources. Finally, real examples of distortion and projective bias are presented, based on a combination pattern of circles and squares. For simplicity detection method labels are shortened, circle centroids are referred to as centroids, conic centroids as conics, checkerboard edge intersections as edges and checkerboard corner saddle refinements are referred to as corners.

4.1 Noise and Blurring

The performance of each method is examined for a range of Gaussian blurring. Fig. 7 shows the mean and standard deviation of the Euclidean errors computed using the true locations. These test image patterns are also projectively transformed so as conic based compensation can be accessed. This shows that the expected detection errors remain relatively constant with respect to blurring. Excluding bias corrupted centroids, these errors are roughly in the pixel range of $0.02 \rightarrow 0.04$, and lower for the edge based method. The robustness of the detection methods to noise is presented in table 2, for additive normally distributed noise. The upper level, $\sigma = 20$ (pix), represents severe noise unlikely to be encountered in typical calibration shots. Typical values for noise in images are in the range $\sigma = 5$ to $\sigma = 10$ pix.

4.2 Positioning

The detection patterns and methods are examined for a range of nine different projective transformations as shown in Fig. 8. The perspective bias of centroid detection on circle patterns can be observed, and increases with perspective severity. These values correspond with their simulated counterparts in Section 3.1.1. These basic statistics do not convey that these errors are not randomly

12

Table 2
Euclidean errors with respect to additive gaussian noises. Errors are compiled over
100 independent trials and are conducted on perspective and distortion free images.

Noise σ (pix) =	Centroids		Conics		Corners		Edges	
	Mean	SD	Mean	SD	Mean	SD	Mean	SD
1	0	0	0.0281	0.0141	0.0051	0.0026	0.0014	0.0007
5	0.0012	0.0039	0.0369	0.0198	0.0144	0.0076	0.0067	0.0035
10	0.0220	0.0122	0.0541	0.0287	0.0279	0.0149	0.0134	0.0070
15	0.0355	0.0188	0.0657	0.0350	0.0420	0.0221	0.0200	0.0104
20	0.0447	0.0233	0.0841	0.0805	0.0568	0.0298	0.0265	0.0139
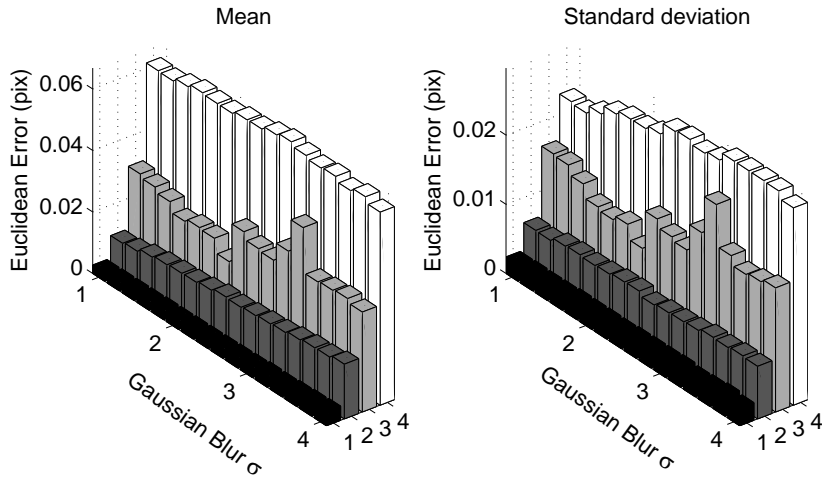
Fig. 7. The mean and standard deviation for the four methods over a range of
gaussian blur levels. 1 $\Rightarrow$ edges, 2 $\Rightarrow$ corners, 3 $\Rightarrow$ conics and 4 $\Rightarrow$ centroids. Images
are subject to a perspective transform.

distributed, and are in fact biased. Fig. 9 shows one sample of this circle
centroid bias compared with bias free adjusted conic fitting.

4.3 Distortion

The patterns and detection methods are evaluated without perspective warp-
ing over the range of distortion levels. External sources of simulation error have
been shown to have insignificant levels in section 2.2. Fig. 10 shows the mean
Euclidean error of circle pattern detection methods steadily increases with
distortion level. This is in excellent agreement with the simulated distortion
bias of section 3.1.2. Edges based detection, because of its line fitting, reduces
distortion bias somewhat, more so for the pincushion variety due to the fixed
windowing size and distortion induced image expansion. Fig. 11 shows the
distortion simulated images, each with associated detection method, for one
sample of distortion.

13
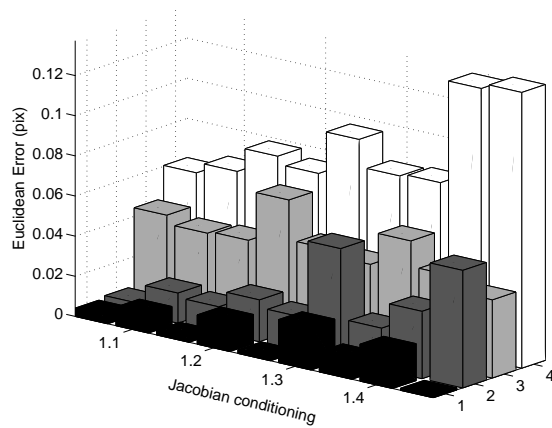
Fig. 8. The mean Euclidean error for the four detection methods ($1 \Rightarrow$ edges, $2 \Rightarrow$ corners, $3 \Rightarrow$ conics, $4 \Rightarrow$ centroids) simulated over various degrees of perspective transforms. Centroid bias is clearly shown by the large mean Euclidean error.
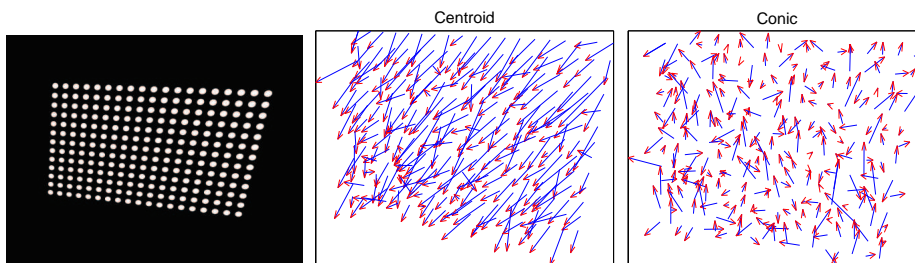

Fig. 9. Sample of one perspective transformation (cond. = 1.25). Vector plots reveal the centroid bias. Residual scale = $\times 2000$.
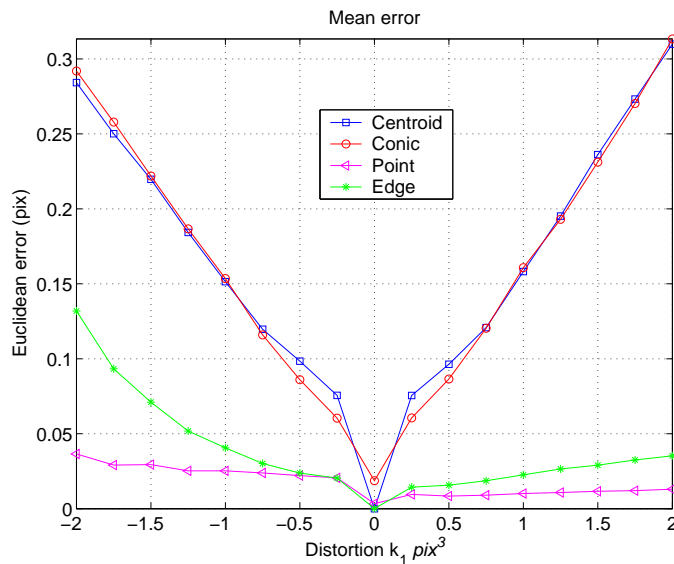

Fig. 10. Illustrates the distortion induced bias in control points for four detection methods.

14
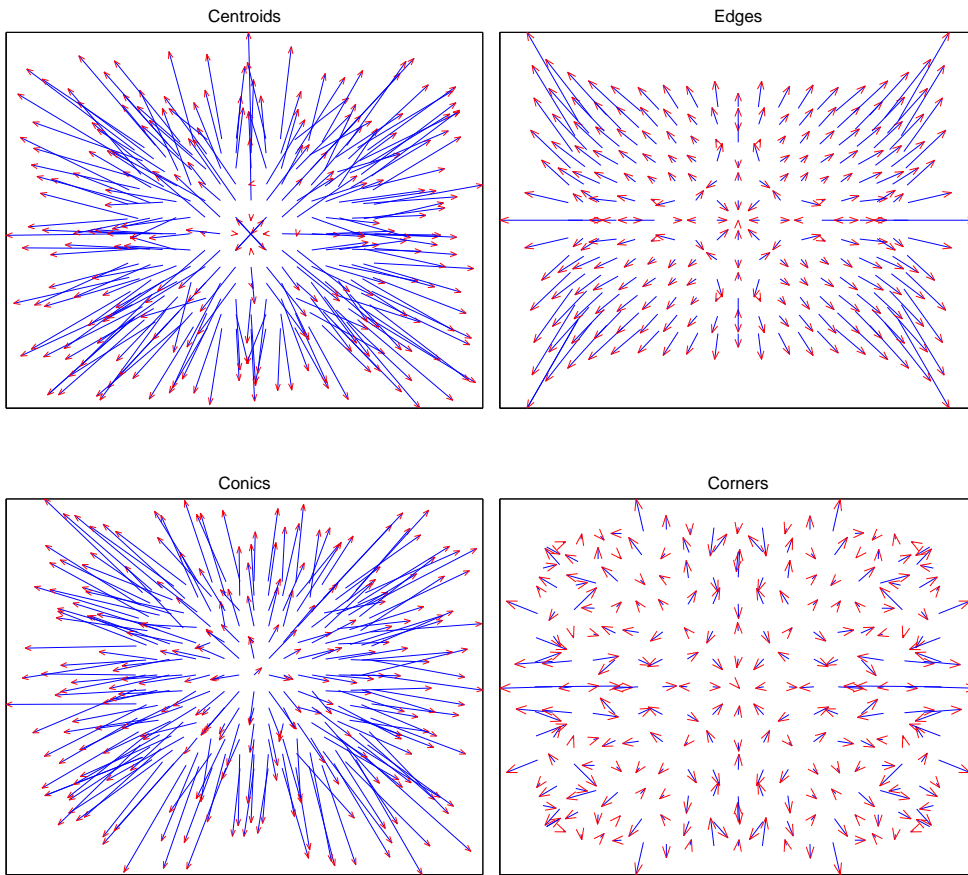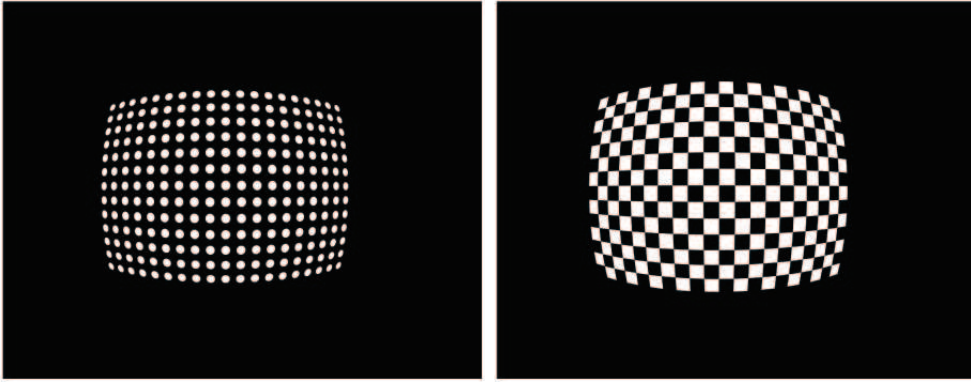
Fig. 11. Left column images show the circle pattern and associated detection method errors. Right column images show the checkerboard and associated methods. Distortion level is $k_1 = -1.5pix^3$. Residual scale $= \times 2000$.

Real examples of bias arising from the use of a particular pattern are shown in Figs. 12 and 13. These show the spatial differences between the centroid and corner based control points, measured by means of a special pattern that combines both circular and square features.
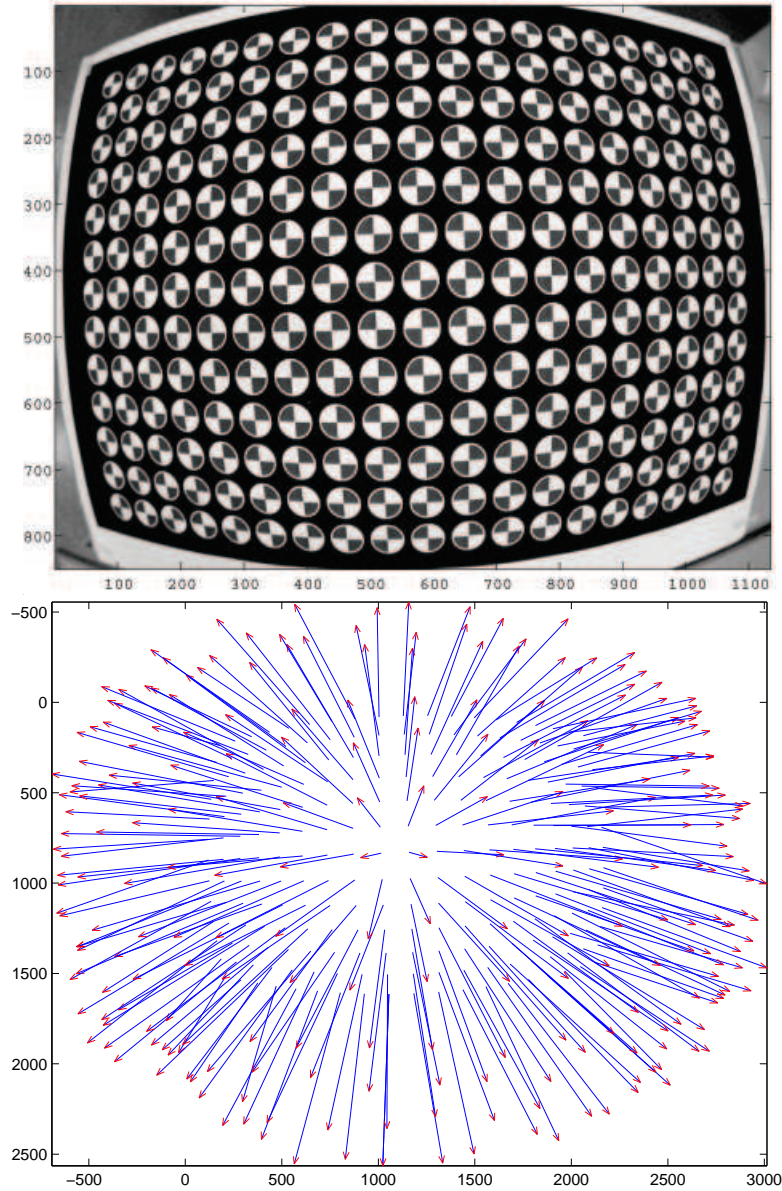

Fig. 12. Example of bias in real image (size: 2272×1704). Circle dia $\simeq 110$ pix, with estimated primary distortion term: $k_1 = -1.2$. Vector plot shows Centroids (uncorrected conics) and Corner differences, revealing the distortion bias (scale is $\times 500$). Residual mean and SD are 1.475(0.322).

Fig. 12 shows an example where an effort was made to minimise perspective distortion (camera was positioned by hand, so undoubtably an element of perspective distortion still remains). As can be observed, the distortion bias is significant. Fig. 13 illustrates a second example including a perspective element. This shifts the apparent center of the bias, but the distortion bias is still dominant. These examples comprehensively demonstrate that such biases are not limited to the simulated case, and equally prevalent in real images.
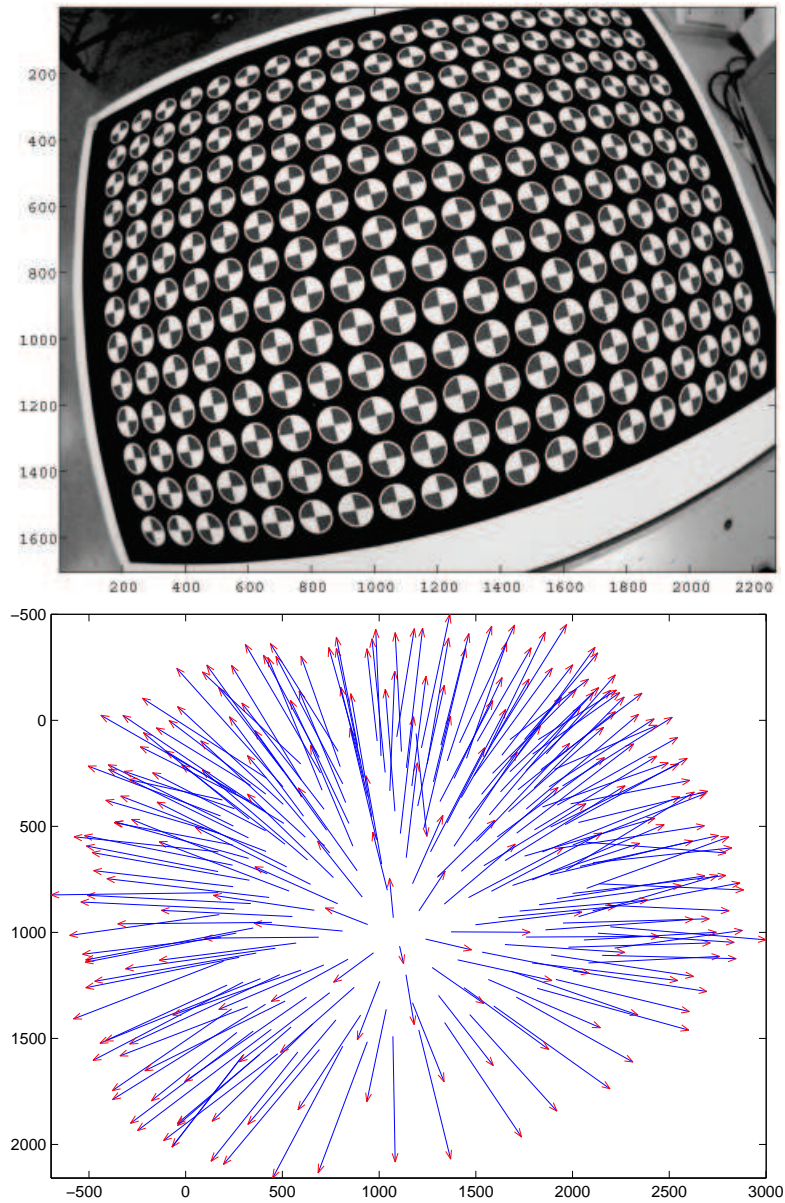

Fig. 13. Example of bias in real image with the same camera and settings as Fig. 12. Vector plot shows Centroids (uncorrected conics) and Corner differences, revealing the almost complete dominance of distortion bias (scale is ×500). Residual mean and SD are 1.272(0.2711).

5 Conclusion

This paper deals with control point recovery from planar calibration charts, by investigating if the choice of pattern can improve the overall detection precision. This accuracy is examined with respect to perspective transformations and lens distortion. Initially, pattern synthesis issues are detailed, in particular the generation of accurate lens distortion in images. Two representative types of patterns are considered: circles and checkerboards, each with two common methods of control point recovery: centroids, conic fitting, edge approximation and corner points. We show theoretically and experimentally that compensated conic fitting, edge approximation and corner points are invariant to perspective bias, while only corner points are invariant to distortion bias. Simulated and real results indicate that distortion induced bias can have a significant magnitude. For a suboptimal circular dot pattern, even a low level of distortion, roughly $\pm 0.3(pix^3)$, will induce much greater distortion bias than the conic estimation error, and is also more significant than the likely perspective bias encountered with normal calibration views. In such cases, the compensation for perspective bias only, is clearly not sufficient to acquire bias free control points. The hierarchy of bias sources for circular type patterns are then, lens distortion, perspective and finally estimation bias. Regarding the practical usage of circular dot patterns, it is recommended that the diameter of the dots are roughly less than ten pixels in order to avoid bias introduction. The results of the study indicate that even well-accepted calibration methods may give poorer results than necessary if applied naively. Overall, this paper highlights these issues in detail and underlines the importance of a correctly designed pattern in camera calibration.

References

Asari, K. V., Kumar, S., Radhakrishnan, D., 1999. A new approach for non-linear distortion correction in endoscopic images based on least squares estimation. IEEE Transactions on Medical Imaging 18 (4), 345–354.

Born, M., Wolf, E., 1980. Principles of Optics, sixth Edition. Permagon.

Hartley, R. I., Zisserman, A., 2003. Multiple View Geometry in Computer Vision, 2nd Edition. Cambridge University Press.

Heikkila, J., 2000. Geometric camera calibration using circular control points. IEEE Transactions on Pattern Analysis and Machine Intelligence 22 (10), 1066–1077.

Jain, R., Kasturi, R., Schunck, B. G., 1995. Machine vision. McGraw-Hill.

Kannala, J., Brandt, S., 2006. A generic camera model and calibration method for conventional, wide-angle and fish-eye lenses. IEEE Transactions on Pattern Analysis and Machine Intelligence 28 (8), 1335–1340.

Li, M., Lavest, J. M., 1996. Some aspects of zoom lens camera calibration. IEEE Transactions on Pattern Analysis and Machine Intelligence 18 (11), 1105–1110.

Lucchese, L., Mitra, S. K., 2002. Using saddle points for subpixel feature detection in camera calibration targets. In: Asia-Pacific Conference on Circuits and Systems. Vol. 2. pp. 191 – 195.

Mallon, J., Whelan, P. F., 2004. Precise radial un-distortion of images. In: International Conference on Pattern Recognition. Vol. 1. pp. 18–21.

Mallon, J., Whelan, P. F., 2005. Projective rectification from the fundamental matrix. Image and Vision Computing 23 (7), 643–650.

Mallon, J., Whelan, P. F., 2007. Calibration and removal of lateral chromatic aberration in images. Pattern Recognition Letters 28 (1), 125–135.

Salvi, J., Armangue, X., Batlle, J., 2002. A comparative review of camera calibrating methods with accuracy evaluation. Pattern Recognition 35, 1617–1635.

Strum, P. F., Maybank, S. J., 1999. On plane-based camera calibration: A general algorithm, singularities, applications. In: IEEE conference on computer vision and pattern recognition. Vol. 1. pp. 432–437.

Tsai, R., 1987. A versatile camera calibration technique for high accuracy 3d machine vision metrology using off-the-shelf tv cameras and lenses. IEEE Journal of Robotics and Automation 3 (4), 323–344.

Weng, J., Cohen, P., Herniou, M., 1992. Camera calibration with distortion models and accuracy evaluation. IEEE Transactions on Pattern Analysis and Machine Intelligence 14 (10), 965–980.

Willson, R., 1994. Modeling and calibration of automated zoom lenses. Ph.D. thesis, Carnegie Mellon University.

Zhang, Z., 1997. Parameter estimation techniques : a tutorial with application to conic fitting. Image and vision computing 15 (1), 59–76.

Zhang, Z., 2000. A flexible new technique for camera calibration. IEEE Transactions on Pattern Analysis and Machine Intelligence 22 (11), 1330–1334.